

## Accepted Manuscript

Experimental and quantum computational study of two new bridged copper(II) coordination complexes as possible models for antioxidant superoxide dismutase: Molecular structures, X-band electron paramagnetic spectra and cryogenic magnetic properties

Yogendra Singh, Ram N. Patel, Satish Kumar Patel, Abhay Kumar Patel, Neetu Patel, Rita Singh, R.J. Butcher, Jerry P. Jasinski, A. Gutierrez

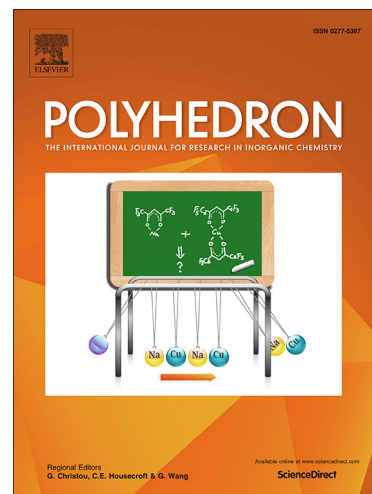
PII: S0277-5387(19)30485-1  
DOI: <https://doi.org/10.1016/j.poly.2019.07.015>  
Reference: POLY 14065

To appear in: *Polyhedron*

Received Date: 1 June 2019  
Revised Date: 12 July 2019  
Accepted Date: 13 July 2019

Please cite this article as: Y. Singh, R.N. Patel, S. Kumar Patel, A. Kumar Patel, N. Patel, R. Singh, R.J. Butcher, J.P. Jasinski, A. Gutierrez, Experimental and quantum computational study of two new bridged copper(II) coordination complexes as possible models for antioxidant superoxide dismutase: Molecular structures, X-band electron paramagnetic spectra and cryogenic magnetic properties, *Polyhedron* (2019), doi: <https://doi.org/10.1016/j.poly.2019.07.015>

This is a PDF file of an unedited manuscript that has been accepted for publication. As a service to our customers we are providing this early version of the manuscript. The manuscript will undergo copyediting, typesetting, and review of the resulting proof before it is published in its final form. Please note that during the production process errors may be discovered which could affect the content, and all legal disclaimers that apply to the journal pertain.



# Experimental and quantum computational study of two new bridged copper(II) coordination complexes as possible models for antioxidant superoxide dismutase: Molecular structures, X-band electron paramagnetic spectra and cryogenic magnetic properties

Yogendra Singh<sup>a</sup>, Ram N. Patel<sup>a</sup>, Satish Kumar Patel<sup>a</sup>, Abhay Kumar Patel<sup>b</sup>, Neetu Patel<sup>b</sup>, Rita Singh<sup>c</sup>, R.J. Butcher<sup>d</sup>, Jerry P. Jasinski<sup>e</sup>, A. Gutierrez<sup>f</sup>

<sup>a</sup>Department of Chemistry, A.P.S. University, Rewa (M.P.) 486003 India

<sup>b</sup> Department of Chemistry, Faculty of Science, The MS University of Baroda, Vadodara 390002, India

<sup>c</sup>Department of Physics, Govt. Model Science College, Rewa (M.P.) 486001 India

<sup>d</sup>Department of Inorganic & Structural Chemistry, Howard University, Washington DC, 22031 USA

<sup>e</sup>Department of Chemistry, Keene State College, 229 Main Street, Keene, NH 03435-2001

<sup>f</sup>Departamento de Química Inorganica, Universidad Complutense, 28040 Madrid, Spain

## Graphical Abstract

Two new bridged copper(II) coordination complexes with NNO donor ligands, *viz.*, [Cu<sub>2</sub>(μ-sulfato)(HL)<sub>2</sub>(H<sub>2</sub>O)].1.5 H<sub>2</sub>O (**1**) and [Cu<sub>2</sub>(μ-succinato)(L)(HL)(H<sub>2</sub>O)]ClO<sub>4</sub> (**2**), where HL/L = *N'*-[(*E*)-pyridin-2-ylmethylidene]benzohydrazide, have been synthesized and characterized using various physico-chemical techniques. Both complexes are structurally characterized using single crystal X-ray diffraction studies and belong to the triclinic crystal system having space group  $P\bar{1}$ .

## Abstract

In the present study, we use a dual approach comprising experimental and quantum computational studies of two new bridged copper(II) coordination complexes with NNO donor ligands, *viz.*, [Cu<sub>2</sub>(μ-sulfato)(L)<sub>2</sub>(2H<sub>2</sub>O)].1.5H<sub>2</sub>O (**1**) and [Cu<sub>2</sub>(μ-succinato)(L)(HL)(H<sub>2</sub>O)]ClO<sub>4</sub> (**2**), where HL/L = *N'*-[(*E*)-pyridin-2-ylmethylidene]benzohydrazide, have been synthesized and characterized using various physico-chemical techniques. Both complexes are structurally characterized using single crystal X-ray diffraction studies. The distances between two copper centers are 3.270(2) Å and 3.178(1) Å, for **1** and **2**, respectively. On the basis of quantum computational DFT study, electronic excitations involve transitions mainly from metal-ligand bonding MO's to the β-LUMO within the dominant Cu atom exhibiting *d<sub>xy</sub>* character and to the β-LUMO + 1. EPR spectra for these polycrystalline samples were determined for the copper(II) hyperfine structures as well their zero-field splitting which are appropriate for the triplet state of such dimers. Cryomagnetic behavior is consistent with weak antiferromagnetic interactions between the Cu(1)⋯Cu(2) centers in both complexes. The magnetic exchange coupling constant (*J*) between the Cu(1)⋯Cu(2) centers for **1** and **2** were determined to be *J* = -1.50(1) and *J* = -7.7(1) cm<sup>-1</sup>, respectively. CH⋯π, π⋯π, and lone pair ⋯π interactions which have gained attention and their role in bimolecular structure analysis has been recognized. In addition, antioxidant superoxide dismutase activity measurements have showed that

homodinuclear complexes give significant scavenging effects against superoxide free radicals. Complex **2** is more antioxidant superoxide dismutase active than **1**.

Keywords: Copper(II)-hydrazone complexes; Molecular structures; Antioxidant superoxide; Cryogenic magnetic properties ; Quantum computational study.

## 1. Introduction

The tridentate coordination mode of hydrazone ligands are very efficient as binucleating ligands for metal ions. Binuclear complexes using tridentate Schiff bases and bridging ligands have been receiving considerable interest due to their biological and industrial relevance[1]. They have received attention as model compounds for the active site of biological copper enzymes[2]. The enzymatic activity of these enzymes is associated with a coordination sphere of the metal active site[3]. Superoxide dismutase (SOD) enzymes are ubiquitous in living systems and serve a vital role in defending oxygen utilizing life forms from oxidative damage[4]. SOD enzymes catalyze the dismutation of superoxide free radical anions, giving rise to a one electron reduction product of molecular oxygen to non-radical products (Scheme 1). The above mentioned features have attracted attention to the design new copper(II) antioxidant biomimetic compounds[5]. The reaction mechanism of a Cu-Zn SOD or a copper(II), biomimetic system consists of a disproportionation of  $O_2^{\cdot-}$  as in the following steps of Scheme 1.

Schiff bases are well known chelating ligands and are used in the synthesis of various mono- bi- and polynuclear metal(II) complexes[6]. The present Schiff base is an NNO donor ligand and acts as a tridentate neutral and mono negative donor for binuclear copper(II) complexes. We have been interested in synthesizing two homodinuclear copper(II) complexes with a specific anion to see the effect of the amide protonation state on the coordination sphere, redox properties and magnetic interactions between the two paramagnetic metal ions[7]. The binding group anions of a sulfate/succinate can act as a 1, 2 bridge and leads to formation of a binuclear complex. It is well known the sulfate/carboxalate groups are able to generate H-bonds leading to formation of a supramolecular architecture which can play an important role in transmission of a magnetic interaction. Both bridging ligands can bridge two metal ions to give rise to a variety of polynuclear carboxalate bridged[7c, 8] and sulfate bridged[9] complexes. The inspiration of this kind of study is not only to know the role of fundamental interactions in both chemical and biological molecular recognition, but also to find out their

potential for technological applications in a number of areas of material science[10]. The Schiff-base used in the present work, is so designed that it can participate in hydrogen bonding interactions. In order to gain insights into the coordination chemistry of such binuclear complexes and an extension of our recent studies in understanding their magnetic behavior, electrochemical and quantum computational density functional studies[7c], we report the synthesis, structural characterization and quantum computational calculations of two binuclear copper(II) complexes  $[\text{Cu}_2(\mu\text{-sulfato})(\text{L})_2(2\text{H}_2\text{O})] \cdot 1.5\text{H}_2\text{O}$  (**1**) and  $[\text{Cu}_2(\mu\text{-succinato})(\text{L})(\text{HL})(\text{H}_2\text{O})]\text{ClO}_4$  (**2**) obtained by a biomimetic synthesis strategy, catalyzing the Cu(II)  $\text{N}_2\text{O}_2/\text{N}_2\text{O}_3$  structural motifs as their inner sphere structure (Scheme 2). Computational density functional theory has been used to predict the most stable geometrical form of the ligand and its complexes. Quantum computational density functional theory also yields significant electronic structural data. In addition, antioxidant assay superoxide dismutase activity data for these complexes was also measured. The coordination site available for the binding of  $\text{O}_2^{\cdot -}$  is clearly shown by the X-ray structures, whereby both have a similar topology.

## 2. Experimental

### 2.1. Materials and methods

Copper(II) sulfate pentahydrate, copper perchlorate hexahydrate, benzoylhydrazide and 2-pyridinecarboxaldehyde were purchased from Aldrich, Qualigens and Across Organics, respectively. All other chemicals were of synthetic grade and used without further purification. Solvents were purified by standard methods before use[11].

**Caution!** Perchlorate salts of metal complexes with organic ligands are potentially explosive. Experiments were carried out at the mmol scale and prepared in small quantities.

### 2.2. Physical measurements

Microanalysis was performed on an Elementar Vario EL III Carlo Erba 1108 analyser. The  $^1\text{H}$  NMR spectrum of the ligand was obtained in  $\text{CH}_3\text{OD}$  with a Bruker Advance 400 (FT-NMR) Instrument. Chemical shifts were reported in parts per million (ppm) using tetramethylsilane (TMS) as internal standard. UV-vis absorption spectra were recorded at room temperature on a Shimadzu UV-vis

recording Spectrophotometer UV-1601 in 1cm quartz cuvettes. The Fourier Transform Infrared (IR) spectra were recorded in KBr on a Perkin-Elmer spectrophotometer in the range 4000-400  $\text{cm}^{-1}$  region. X-band electron paramagnetic resonance (EPR) spectra were measured with a Varian E-line Century Series (X-band 9.1 GHz) Spectrometer equipped with a dual cavity and operating at X-band with 100 kHz modulation frequency. Varian quartz tubes were used for measuring EPR spectra of polycrystalline samples and frozen solutions. Tetracyanoethylene (TCNE) was used as a marker ( $g_e = 2.00277$ ). Cyclic voltammetry measurements were performed on solutions containing 0.1 mol  $\text{L}^{-1}$  tetrabutyl ammonium perchlorate (TBAP) with a BAS-100 Epsilon Electrochemical Analyzer having an electrochemical cell with a three-electrode configuration. Ag/AgCl was used as a reference electrode, glassy carbon as the working electrode and platinum wire as an auxiliary electrode. The concentrations of the complexes used for redox potential measurements were  $3 \times 10^{-3}$  M DMSO solutions. All measurements were carried out at room temperature under nitrogen atmosphere. Ferrocene (Fe) was added to the solution as an internal standard. Molar conductivities of freshly prepared complexes  $3 \times 10^{-3}$  M DMSO solutions were measured on a Systronics conductivity TDS meter.

### 2.3. Cryogenic magnetic susceptibility studies

The variable temperature magnetic susceptibility of complexes **1** and **2** were measured by using a Quantum Design SQUID magnetometer MPMS-XL5 with liquid helium cryostat in the temperature range of 2-300 K at an applied field of 0.1 T. All data were corrected for the diamagnetic correction done by using Pascals constants. The Magnetic susceptibility data were fitted with least-square techniques. The experimental data were also corrected for temperature independent paramagnetism (TIP) of the metal center.

### 2.4. X-ray crystallography

X-ray diffraction data were performed on Bruker APEX-II diffractometer using graphite monochromated Mo- $K\alpha$  radiation ( $\lambda = 0.71073 \text{ \AA}$ ). Crystals suitable for single crystal X-ray analysis of all complexes were grown by slow evaporation of the reaction mixtures at room temperature. Single-crystals suitable for single-crystal X-ray analysis were mounted on glass fibers and used for data collection. The crystal orientation, cell refinement, and intensity measurements were made using a CAD-4PC performing  $\Psi$ -scan measurements. The structures were solved by direct methods by using SHELXT[12] and refined with SHELXL-2014[13]. All non-hydrogen atoms were refined

anisotropically by full-matrix least squares. All hydrogen atoms were located in difference Fourier maps and allowed to refine using a riding model.

## 2.5. Quantum computational density functional theory

All quantum computational calculations were performed using the GUASSIAN09 package program[14] by the DFT/B3LYP method. The input files of the copper(II) complexes were prepared with Gauss View 5.0.9[15]. In the computational model, the anion was ignored and the cationic complexes were taken into account using crystallographic data as starting input. Time dependent quantum computational DFT calculations were performed and compared to the electronic spectra of complexes with the LANL2DZ basis set in the gas phase[16]. Vertical electronic excitations based on B3LYP optimized geometries were computed using the time dependent density functional theory (TD-DFT) formalism[17] in DMSO using a conductor-like polarizable continuum model[18].

## 2.6. Antioxidant superoxide dismutase (SOD) assay

The *in-vitro* antioxidant superoxide dismutase (SOD) activity was measured using alkaline DMSO as a source of the superoxide radical ( $O_2^{\cdot-}$ ) and the SOD activity was evaluated using the nitro blue tetrazolium (NBT) method[19]. A unit of antioxidant SOD activity is the concentration of the complex, which causes 50% ( $IC_{50}$ ) inhibition of alkaline DMSO and mediated reduction of NBT. The catalytic rate constants were calculated as  $k_{MCCF} = k_{NBT} [NBT] / IC_{50}$ , where  $k_{NBT}$  (pH = 7.8) =  $5.94 \times 10^4 M^{-1} S^{-1}$ [20].

## 2.7. Synthesis of the ligand

The Schiff base was prepared by a standard literature procedure[21] and synthesized by reacting benzoylhydrazide (136.1 mg, 10.0 mmol) and 2-pyridenecarboxaldehyde (107.1 mg, 10.0 m mol) in ethanol. The resulting solution was refluxed for 4 hours during which a brown precipitate was formed (Scheme 3). The reaction mixture was then cooled to room temperature and the solid formed was filtered and washed with ethanol. The product was recrystallized from hot ethanol. Yield: (83%).

Anal. Calcd for  $C_{13}H_{11}N_3O$  (%): C, 69.32; H, 4.92; N, 18.66. Found (%): C, 69.31; H, 4.92; N, 18.65. IR data (KBr disc,  $cm^{-1}$ ): 3438, 2920, 2852, 1970, 1595, 1456, 1379, 1324, 1253, 1154, 1102, 1030, 763, 703 and 651 (Fig. S1).  $^1H$  NMR ( $CH_3OD$ ): 3.31(s, 1H, OH); 7.39–8.56 (m, 9H, Ar-H) [Fig. S2].

## 2.8. Synthesis of complexes

### 2.8.1. Synthesis of $[\text{Cu}_2(\mu\text{-sulfato})(\text{L})_2(2\text{H}_2\text{O})]\cdot 1.5\text{H}_2\text{O}$ **1**

To a MeOH solution (20 mL) of  $\text{CuSO}_4\cdot 5\text{H}_2\text{O}$  (0.250 g, 1.0 mmol) was added a MeOH solution (20 mL) of the ligand (0.500 g, 2.0 mmol) with stirring for 30 min at 25°C. The resulting green solution was allowed to slowly concentrate by evaporation at room temperature for a period of one week to yield a green solid. A green microcrystalline solid deposited was collected by filtration, washed with methanol and stored in  $\text{CaCl}_2$  desiccator at RT. Yield: 70%; Anal. Found (%): C, 43.51; H, 3.62; N, 11.57; Calcd (%) for:  $\text{C}_{52}\text{H}_{50}\text{Cu}_4\text{N}_{12}\text{O}_{17}\text{S}_2$ : C, 43.53; H, 3.52; N, 11.73; IR data (KBr disc,  $\text{cm}^{-1}$ ): 3440, 2920, 2853, 1628, 1464, 1437, 1381, 1316, 1285, 1105, 1022, 748, 697, 660, 572, 511 and 443 (Fig. S3). Electronic absorption spectra in DMSO [ $\lambda_{\text{max}}$ , nm ( $\epsilon$ ,  $\text{M}^{-1}\text{cm}^{-1}$ ): 704(30), 390 (7100). Molar conductivity ( $\Lambda\text{M}$ ) 17  $\Omega\text{cm}^{-2}\text{mol}^{-1}$  in DMSO solution.

### 2.8.2. Synthesis of $[\text{Cu}_2(\mu\text{-succinato})(\text{L})(\text{HL})(\text{H}_2\text{O})]\text{ClO}_4$ **2**

To a MeOH solution (20 mL) of  $\text{Cu}(\text{ClO}_4)_2\cdot 6\text{H}_2\text{O}$  (0.642 g, 1.0 mmol) was added a MeOH solution (20 mL) of ligand (HL) (0.500 g, 2.0 mmol). The resulting green solution was stirred with succinic acid (0.118g, 1.0 mmol) and a few drops of triethyl amine were added to give a dark green solution. The dark solution was allowed to slowly concentrate by evaporation at room temperature for 3 days. Dark green microcrystalline crystals were deposited and collected by filtration, washed with methanol and stored in  $\text{CaCl}_2$  desiccator at RT. Yield: 72%; Anal. Found (%): C, 44.41; H, 3.49; N, 10.34; Calcd (%) for:  $\text{C}_{30}\text{H}_{28}\text{ClCu}_2\text{N}_6\text{O}_{11}$ : C, 44.42; H, 3.47; N, 10.36. IR data (KBr disc,  $\text{cm}^{-1}$ ): 3856, 3750, 3447, 3067, 2927, 2860, 2715, 2613, 2427, 2364, 2075, 1593, 1489, 1323, 1271, 1153, 1101, 996, 763, 703, 660 and 655 (Fig. S4). Electronic absorption spectrum in DMSO [ $\lambda_{\text{max}}$ , nm ( $\epsilon$ ,  $\text{M}^{-1}\text{cm}^{-1}$ ): 712(38), 390 (6300). Molar conductivity ( $\Lambda\text{M}$ ) 125  $\Omega\text{cm}^{-2}\text{mol}^{-1}$  in DMSO solution.

## 3. Results and discussion

### 3.1 Synthesis of HL, **1** and **2**

Both copper(II) complexes were synthesized from the reaction of a copper(II) salt with a Schiff base ligand (HL). The target complexes were first characterized by elemental analysis followed by a conventional solution method for the synthesis and formation of crystalline products suitable for single-crystal X-ray diffraction analysis. The synthetic routes of the ligand and its corresponding binuclear copper(II) complexes are described in Scheme 4. After 3-6 days, crystals of **1** and **2** suitable for single-crystal X-ray analysis were isolated. The IR spectra of complexes **1** and **2** display IR absorption bands at 1595 and 1590  $\text{cm}^{-1}$  respectively, (Fig. S3, S4) which can be assigned to the  $\nu(>\text{C}=\text{N})$  of the coordinated ligand (HL/L), whereas for the free ligand (HL) the same band is observed at 1628  $\text{cm}^{-1}$ . The shift of this

band on complexation towards lower wave numbers indicates the coordination of the azomethine nitrogen ( $>C=N$ ) to the copper centre[22]. In both complexes intense absorptions of sulfato **1** and succinato bridges stretching vibrations at 1379 and 1378  $\text{cm}^{-1}$  respectively[23]. Complex **2** shows an absorption band at 1488  $\text{cm}^{-1}$  which could be assigned to  $HC=N-C-O^-$  moiety of a deprotonated ligand [24]. The molar conductivity value for complex **1** in DMSO solution ( $3 \times 10^{-3} \text{mol L}^{-1}$ ) was  $17 \Omega \text{cm}^2 \text{mol}^{-1}$  indicating non-electrolytic behavior[25]. However, complex **2** shows a molar conductivity ( $\Lambda M$ ) of  $125 \Omega \text{cm}^2 \text{mol}^{-1}$  in DMSO solution corresponding to a 1: 1 electrolyte[25, 26].

### 3.2. X-ray crystallography structural characterization of complexes 1 and 2

The molecular structures of both complexes were crystallographically characterized and the structures are shown in Fig. 1a. Selected structural parameters are presented in Table 1 and important bond distances and angles are shown in Table 2. Both complexes are binuclear in nature.

In complex **1** two oxygen atoms from sulfate anion and two oxygen atoms from carbonyl moiety of the Ligand(HL), act as bridging units. In this complex Cu1 is square pyramidal and Cu2 is hexacoordinated. The basal plane of the Cu1 centre is occupied by a Schiff base ligand and one oxygen (O1) atom of a sulfate anion, thus completing a square pyramidal structure. The distortion index ( $\tau_5$ ) for a pentacoordinated Cu1 centre can be estimated by Addison distortion index ( $\tau_5$ ) as  $\tau_5 = (\beta - \alpha / 60^\circ)$ [27], in which  $\beta$  and  $\alpha$  are two largest coordinating angles, and  $\tau = 0$  for ideal square pyramidal and  $\tau = 1$  for ideal trigonal pyramidal geometry. The estimated  $\tau_5$  value for this centre is 0.16, indicating distortion in five coordinate geometry. For the Cu2 centre the degree of distortion from octahedral coordination can be defined through a tetragonality parameter (T) as:  $T = R_{\text{int}}/R_{\text{out}}$ , in which  $R_{\text{int}}/R_{\text{out}}$  are the average in plane and out plane bond distances respectively and a T value  $< 0.9$ , indicates static and  $T = 1$  dynamic distortion in octahedral geometry[28]. The degree of distortion the geometry around Cu2 was estimated to be 0.78. Therefore, the geometry around Cu2 is ascribed as a static distortion. The Cu...Cu distance (3.270(1) Å) is comparable to that of reported complexes[29]. The

copper(II) coordination sphere of **1** is shown in Fig. 1b. Models of this complex constitute infinite 1-D chains along the b-axis through hydrogen bonds involving the C-H groups of HL and free coordinated water molecules (Fig. 1c). Two adjacent units are connected by such hydrogen bondings. Distances of various hydrogen bonds and weak intermolecular interactions are summarized in given in Table 3. These hydrogen bonds and weak intermolecular interactions (C6-H6BA...O2W, O2W-H2W2...O1W and O1W-H1W1...N3B) for one  $R_3^3(8)$ , graph-set ring motif Similarly (C6B)-H6BA...O2W, O2W-H2W2...O1W and O1W-H1W1...N3B for other  $R_3^3(8)$ ) results in a dimer like association between pairs of complexes in an extended two heterosynthon (motif)  $R_3^3(8)$  graph-set ring motif in Fig.1c. These types of distances and angles are generally employed to describe the unusual molecular shape a complex has that is determined from a complex system of inter- and intramolecular non-covalent interactions comprising face-to-face and edge-to-face aromatic interactions as well as lone pair interactions[30]. Additional stabilization of these motifs is provided by the above non-covalent interactions. Crystal packing is further supported by additional weak  $\pi \cdots \pi$  stacking interactions and CH... $\pi$  inter- and intramolecular contacts. Two pairs of weak intermolecular interactions are present between a CH group from the benzoyl rings (C13A--H13A and C13B--H13B) with  $\pi$  electrons of the pyridyl rings (Fig.1c), with distances 2.941 (15) Å and 3.334 (16) Å, respectively, while a CH... $\pi$  intermolecular contact remains between the C4B--H4B group of a pyridyl ring and the  $\pi$  electrons of nearby benzoyl rings with a distance of 3.501(14) Å. Chelate rings of metal complexes with delocalized  $\pi$  electrons can be involved in non-covalent interactions in similar ways to aromatic molecules. In the presence of a chelate ring with delocalized  $\pi$  electrons there is a close contact between a copper atom and a carbon atom from nearby benzoyl rings. This contact survives between a C6B--H6BA group from a benzoyl ring with a chelate ring of the complex with distance of 3.535(13) Å. Inter- and intramolecular H... $\pi$  interactions from H1W1/H1W2 and  $\pi$  electrons from nearby chelate rings, with distances displayed, are shown in Fig. 1d. Crystal packing is also affected by  $\pi \cdots \pi$  stacking interactions between planar molecular units and are formed due to a stacking of the molecular chains. These interesting observations involving molecules from complex **1**, therefore, exhibit effective  $\pi \cdots \pi$  (aryl-aryl, aryl-metal chelates and metal chelate-metal chelates) stacking interactions. Regarding intermolecular stacking, a pair of pyridyl-benzyl stacking interactions are observed with a centeroid-centeroid distance,  $d_{C-C} = 3.989$  Å. Along with these intermolecular interactions, an additional metal-aryl ring  $\pi \cdots \pi$  stacking interaction is observed with a distance,  $d_{C-C} = 4.515$  Å. So, the metallo aromaticity in these types of aryl chelate rings has been structurally characterized[31]. In this complex intermolecular  $\pi \cdots \pi$  (aryl-aryl, aryl-metal chelates and

metal chelate-metal chelates) are also observed with distances,  $d_{C-C} = 4.331 \text{ \AA}$  and  $d_{C-C} = 4.298 \text{ \AA}$ . Many of these types of contacts can be seen in Fig. 1(e). Uncoordinated solvent molecules and long pairs from the oxygen atom of coordinated water molecules with metal chelates along with lone pair interactions is also shown in Fig. 1(f). Recently lone pair (lp)  $\cdots \pi$  interactions have gained renewed attention and their role in bimolecular structure is being recognized[32].

The molecular structure of complex **2** is shown in Fig. 2a. The structure consists of a succinate group, two HL and copper(II) binuclear cations and one perchlorate anion. The carbonyl oxygen atoms of HL link the binuclear units, in a bis(monodentate) way, building one-dimensional chains of Cu(II) linked by succinate and carbonyl groups from HL as spacers. They are assembled in a three-dimensional network. The selected bond lengths and angles are given in Table 3. In this complex Cu1 is in a distorted octahedral geometry and coordinated to four oxygen atoms and two nitrogen atoms. The degree of distortion (T) is 0.79, which indicates static distortion in the geometry [28]. The Cu2 centre has distorted square pyramidal geometry with a distortion index  $\tau_5 = 0.23$ , showing distorted square pyramidal geometry around the Cu2 centre. The distances of four equatorial bonds Cu2-N2B, Cu2-O1B, Cu2-O2 and Cu2-N1B are 1.922(3), 1.969(3), 1.922(3), and 2.008(3)  $\text{\AA}$ , respectively. However, the axial bond distance Cu2-O1A was found to be somewhat longer. The copper(II) coordination sphere of **2** is presented in Fig. 2b. The Cu  $\cdots$  Cu distance (3.270(1)  $\text{\AA}$ ) is comparable to that of **1** and other similar reported complexes[29]. In the asymmetric unit, the cationic and perchlorate anion are linked by internuclear hydrogen bonds, where the O1W-H1W1  $\cdots$  Cl1 and O1W-H1W1  $\cdots$  O12 interactions involving the H atoms of bonded water molecules of one binuclear complex from a pair of bifurcated donor bonds yielding a heterosynthon (motif) with a  $R_1^2(3)$  graph-set ring motif. The O1W-H1W1  $\cdots$  O12 and O1W-H1W1  $\cdots$  Cl1 interactions (involving an H atom of a coordinated water molecule of an adjacent binuclear unit) together form a pair of donor bonds defining the heterosynthon (motif)  $R_1^2(3)$  graph-set ring motif. Similarly, two more heterosynthon (motif)  $R_2^2(8)$  graph-set ring motifs are constituted by two binuclear units into a three dimensional network by a collection of O1W-H1W2  $\cdots$  N3A, C6A-H6AA  $\cdots$  O12, O1W-H1W  $\cdots$  O12 and O1W-H1W  $\cdots$  Cl1 hydrogen bonds and weak intermolecular interactions. These interactions are displayed in Fig. 1c. A careful analysis of the crystal

packing also revealed that  $\text{CH}\cdots\pi$ ,  $\pi\cdots\pi$  and lone pair  $\cdots\pi$  interactions are an additional feature of this complex. In complex **2**, in addition to hydrogen bonding interactions, further several non-covalent interactions *viz.*, weak  $\text{CH}\cdots\pi$ ,  $\text{H}\cdots\pi$ ,  $\pi\cdots\pi$  and lone pair  $\cdots\pi$  interactions similar to complex **1** have been observed. These interactions are shown in Fig. 2 (d-f) and distances of different non-covalent interactions as well as an extended network of weak  $\pi\cdots\pi$  stacking interactions between nearby benzyl and pyridine rings including the centeroid-centeroid distances of the  $\pi\cdots\pi$  stacking interactions are presented in Table S1. Both complexes exhibit similar intramolecular stacking parameters and they are appropriate enough to consider that effective "metal chelate-aryl rings" exhibiting weak  $\pi\cdots\pi$  stacking interactions are operative. Such intramolecular "metal chelate-aryl rings"  $\pi\cdots\pi$  stacking represent new structural evidence of the metalloaromaticity. In addition, these complexes show different molecular structural patterns to recognize themselves and build upon the crystal packing. A further interesting observation is that in both complexes inter- and intramolecular  $\pi\cdots\pi$  and  $\text{CH}\cdots\pi$  stacking interactions coexist with extensive weak 3-D hydrogen bonding intermolecular interaction network. Uncoordinated perchlorate ions are shown in Fig. 2(f) which is responsible for additional weak interactions to form these supramolecular structures. Oxygen atoms of coordinated water molecules showed lone pair of interactions with metal chelates (Fig. 2(f)). Studies on lone pair (lp) $\cdots\pi$  interactions and their importance in biomolecular structures have already been reported [33]. Although, the nature of (lp) $\cdots\pi$  interactions in general are weak and attractive.

### 3.3. Cryogenic magnetic properties

The susceptibility of both complexes has been measured in the range 2-300 K. The temperature dependence of  $\chi$  and  $\chi T$  for complexes **1** and **2** are shown in Fig. 3 and Fig. 4, respectively. The  $\chi T$  room temperature value for **1** per dimeric unit is  $0.83 \text{ cm}^3\text{Kmol}^{-1}$  and corresponds to a total magnetic moment of  $2.57\beta$ , typical for two non interacting  $S = \frac{1}{2}$  ions. This value is kept approximately constant on lowering the temperature to 30 K and then abruptly decreases to a minimum value of  $0.556 \text{ cm}^3\text{Kmol}^{-1}$  at 2 K. This behaviour is consistent with an antiferromagnetic interaction between the copper ions in the dinuclear compound and can be interpreted by using the spin Hamiltonian  $H = -J\cdot S_1\cdot S_2$ , whose analytical expression is the well-known Bleaney-Bowers equation[34].

$$\chi = Ng^2\beta^2 / kT \cdot \frac{2}{3 + e^{-J/kT}} \quad (1)$$

where  $N$ ,  $g$ ,  $\beta$  and  $k$  have their usual meaning and  $J$  is the coupling constant between the two interacting copper spins. The best fit has been obtained for  $g = 2.102(3)$  and  $J = -1.50(1) \text{ cm}^{-1}$ , with  $R^2 = 0.9974$  (Fig.3).

These data are indicative of a small coupling between the two copper ions. The crystal structure supports this weak interaction since the coupling path through one bridging oxygen involves a long Cu–O distance product of the Jahn-Teller distortion in the Cu(II) coordinative environment. The theoretical magnetic orbitals for both complexes **1** and **2** are shown in Scheme 5.

The magnetic behaviour of **2** is similar to that of complex **1**. It shows a room temperature  $\chi T$  value of  $0.587 \text{ cm}^3\text{Kmol}^{-1}$  per dimeric unit, somewhat lower from the expected value for two copper ions. This value slightly increases to  $0.596 \text{ cm}^3\text{Kmol}^{-1}$  at 250 K, a fact probably due to some error in the experimental values. On lowering the temperature, the  $\chi T$  value steadily decreases to  $0.478 \text{ cm}^3\text{Kmol}^{-1}$  at 25 K followed by a drop to  $0.0375 \text{ cm}^3\text{Kmol}^{-1}$  at 2 K. The behaviour between 25 and 250 K can be interpreted as a contribution of a temperature independent paramagnetism [35], while the drop at lower temperatures is indicative of the antiferromagnetic coupling expected for the two copper ions present in the molecule.

The room temperature  $\chi T$  value found for this compound corresponds to a magnetic moment of  $2.17 \beta$ , lower than the predicted value of  $2.44 \beta$  for two uncoupled  $S = \frac{1}{2}$  spins. The interacting binuclear magnetic cluster does not give any substantial fit of data (with some errors), so it may be assumed that intercluster interaction, if any, must be very small. Based on this assumption, the paramagnetic susceptibility has been considered as the sum of the copper dimer contribution (represented by equation 1) and a temperature independent paramagnetism. The best fit of the data below 250 K gave  $g = 2.070(2)$ ,  $J = -7.7(1) \text{ cm}^{-1}$ ,  $\text{TIP} = 290(6) \times 10^{-6} \text{ cm}^3\text{mol}^{-1}$ , with  $R^2 = 0.9969$  (Fig.4). No significant changes were observed on fitting the  $\chi T$  values between 2 and 300 K.

The fitting of the susceptibility variation using the same parameters (Fig.4 inset) reproduces well the maximum observed at 8 K, a consequence of the antiferromagnetic coupling between the copper atoms. This maximum is not observed for **1** since the smaller coupling constant

would shift it to  $\sim 2$  K, the lower limit of the measurements. These fittings indicate that both dimers have a similar magnetic behavior, differing only in a somewhat more intense coupling for **2**. There are two short Cu–O distances (1.97 and 1.99 Å in both derivatives) and two long ones (2.47 and 2.74 Å for **1** and 2.38 and 2.70 Å for **2**), leading to a Cu–Cu distance of 3.27 Å and 3.18 Å, respectively. The shorter distances in **2** could account for the observed higher  $J$  value. Alternatively, a three atom bridge path (Scheme4) is possible, since both copper atoms are bridged by one sulfate anion in **1** and one carboxylate in **2**. Never the less, this path is less prone to be responsible for the magnetic coupling, but it could have an indirect influence, since the smaller size of the O–C–O fragment relative to the O–S–O fragment should be responsible for the shorter distances found in **2**.

### 3.4. Electronic spectral studies

The electronic spectra of complexes **1** and **2** have been recorded in DMSO solutions. The UV-visible spectrum of complexes **1** and **2** ( $3 \times 10^{-3}$  M) in DMSO shown in Fig. S3 indicates a broad d–d band at 704 nm for **1** and at 712 nm for **2**. In the visible region, each spectrum involves ligand field bands, appearing in the  $\sim 700$  nm regions, corresponding to transitions  $d_{z^2} \rightarrow d_{x^2-y^2}$  and  $d_{xz}$ ,  $d_{yz} \rightarrow d_{x^2-y^2}$ , respectively, as expected for square-planar Cu(II) complexes and confirming the  $d_{x^2-y^2}$  based ground state[36]. Square-planar Cu(II) complexes may be formed by the decomposition or dissociation of complexes to mononuclear species in DMSO, as expected for Square-planar environment around Cu(II) centre. Such types of absorption bands between the Cu(II)–Cu(II) homobinuclear copper(II) complexes were observed in homobinuclear complexes reported in the literature[37]. In addition, the UV-visible spectra of both complexes at 390 nm are attributed to a L  $\rightarrow$  M charge transfer associated with the nitrogen and oxygen donors [38] as shown in Fig. S5.

### 3.5. EPR Experiments

The EPR spectra of complexes **1** and **2** in polycrystalline material at RT and in DMSO solutions ( $3 \times 10^{-3}$  M) at LNT are recorded and shown in Fig. 5. The estimated EPR parameters are presented in Table 4. The EPR spectra of complexes **1** and **2** in polycrystalline are typical of  $S = 1$  systems. The polycrystalline EPR spectra of both complexes were recorded at room temperature (RT) and are displayed in Fig. 5. The room temperature polycrystalline spectra exhibit the expected spectral features

of a triplet state with a low field ( $\Delta M_s = \pm 2$ ) signal [39]. The spin Hamiltonian parameter ( $\mathcal{H}$ ) for an  $S = 1$  state interacting with a magnetic field (H) is defined as:

$$\mathcal{H} = g\beta H_s + DS_z^2 + E(S_x^2 - S_y^2) - (2/3)D$$

where D and E are zero field splitting parameters. The polycrystalline spectra of binuclear complexes **1** and **2** are quite similar in appearance (Fig. 5), with parallel and perpendicular signals unresolved at X-band frequencies. The EPR spectra are in agreement with the geometry confirmed from molecular structures (Fig. 1(a) and 2(a)). The EPR spectrum of complex **1** consists of a  $g_{\parallel}$  absorption at  $g = 2.237$  and a signal corresponding to  $g_{\perp}$  signal at  $g = 2.060$ . Similar spectral features were also shown by complex **2**. The half-field  $\Delta M_s = \pm 2$  transitions near 1560 G for both complexes are present in EPR spectra. This signal is comparatively strong in complex **2** [Fig. 5(b)]. These kinds of observations at RT suggest that the two copper(II) ions are antiferromagnetically spin-spin coupled, as demonstrated through variable temperature magnetic measurements[40]. The exchange interaction parameter G, of complexes (3.410 for **1** and 2.924 for **2**) suggest that there is an exchange interaction between two copper centers which may be propagated through bridging contacts as shown in molecular structures [41]. Zero- field splitting parameter (D) of present complexes shown in Table 4 and are consistent with other reported binuclear copper(II) complexes [39]. Unfortunately, the forbidden transition ( $\Delta M_s = \pm 2$ ) is not defined in **1** and poorly resolved in **2** DMSO solution at LNT. It may be caused by the decomposition or dissociation of complexes to mononuclear species in DMSO, as a result EPR spectra in DMSO at LNT are typical for usual mononuclear copper(II) complexes with square planar geometry[42]. EPR spectra of both complexes exhibit three  $g_{\parallel}$  lines well-defined and one overlapped with  $g_{\perp}$  component at high field part of the spectra at LNT [Fig. 5]. EPR spectra of both complexes **1** and **2** were also recorded in DMSO solution at RT in both cases poorly resolved forbidden transition ( $\Delta M_s = \pm 2$ ) was observed (Fig. S6 and S7). The symmetric shape of spectra with a narrow high field peak ( $g_{\perp}$ ) and low field components ( $g_{\parallel}$ ) is a characteristic for a g-factor anisotropy with  $g_{\parallel} > g_{\perp}$ , where indicates  $\parallel$  and  $\perp$  denote the direction of the magnetic field parallel and perpendicular to the anisotropy axis. The values of  $g_{\parallel}$  and  $g_{\perp}$  of complex **1** and **2** are consistent with a  $d_{x^2-y^2}$  based ground state[43]. EPR parameters and d-d transition energies were used to estimate in-plane,  $\sigma$ -bonding parameters ( $\alpha^2$ ), in-plane-  $\pi$  ( $\beta^2$ ) and out-of plane-  $\pi$  ( $\gamma^2$ ) parameters, which may be known as

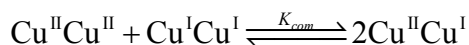
measures of co-valency in metal complexes. The values of these parameters are consistent with strong in-plane  $\sigma$  and in-plane  $\pi$ -bonding. The orbital reduction factors ( $K_{\parallel}$  and  $K_{\perp}$ ) were also evaluated in the present complexes  $K_{\parallel}$  value is less than  $K_{\perp}$  in both complexes employs considerable in-plane bonding.

### 3.6. Electrochemical studies

The redox behavior of these complexes was studied using cyclic voltammetry (CV) and differential pulse voltammetry (DPV). Cyclic voltammograms of **1** and **2** in DMSO ( $3 \times 10^{-3}$  M) were recorded at ambient temperature with TBAP as a supporting electrolyte (0.1M) in a nitrogen atmosphere. Cyclic voltammograms (scan rate 300 mv/s) are shown in Fig. 6(a) and redox properties are summarized in Table 5. In both complexes two reduction processes ( $\text{Cu}^{\text{II}}\text{Cu}^{\text{II}} + e^- \rightarrow \text{Cu}^{\text{II}}\text{Cu}^{\text{I}}$  and  $\text{Cu}^{\text{II}}\text{Cu}^{\text{I}} + e^- \rightarrow \text{Cu}^{\text{I}}\text{Cu}^{\text{I}}$ ) vs. Ag/AgCl references, both involving an identical number of electrons, are revealed from DPV experiments (Fig. 6b). It has been observed that DPV is a very good technique for resolving redox responses having small differences in peak potentials, provided the two peaks differ in their formal potential by more than 180 mV. The Cu(II)/Cu(I) couple appears at  $\sim 0.018$  V with respect to the Ag/AgCl electrode and in most cases in the CV experiments the two Cu(II)/Cu(I) couples are not resolved, though in DPV these two couples are sometimes resolved. The cyclic voltammograms for both **1** and **2** were also recorded in acetonitrile (Fig. S8). In acetonitrile some differences appear in redox behaviour which may associated with changes in the coordination spheres of complexes **1** and **2**. The difference in electrochemical behaviour in both complexes could be due to the distribution of the electron density of coordination sphere.

A comparison of the electrochemical data (Table 5) of these complexes indicates that process I in **1** and **2** is due to a one-electron  $\text{Cu}^{\text{II}}\text{Cu}^{\text{II}} \rightleftharpoons \text{Cu}^{\text{II}}\text{Cu}^{\text{I}}$  reduction the involving the square planar copper site, while the reduction  $\text{Cu}^{\text{II}}\text{Cu}^{\text{I}} \rightleftharpoons \text{Cu}^{\text{I}}\text{Cu}^{\text{I}}$  at more negative potential (Process II) also involves a square planar copper center [44]. The oxidation potentials of complex **1** are more negative than **2** and

could be due to some structural changes involved [Fig. 1(a) and 2(a)]. Reduction potentials for complexes **1** and **2** are in agreement with reported binuclear complexes in the literature[45]. The reduction process of complexes **1** and **2** were irreversible in these reduction processes where two electrons are involved. The redox process of two copper centers seems to occur over a broad range with two reduction and oxidation peaks (Fig. 6a). These reduction waves are confirmed by DPV experiments (Fig. 6b). The stability of the mixed valent complexes is expressed by the conproportionation constant ( $K_{con}$ ) for the following equilibrium:



which was estimated using the relationship  $\log K_{con} = 16.9(\Delta E_{1/2})$ [46]. The observed value of  $K_{con}$  for both complexes is given in Table 5. From Table 5, it is evident that the large  $K_{con}$  values indicate that the addition of a second electron is most difficult than the first electron and the  $\text{Cu}^{\text{II}}\text{Cu}^{\text{I}}$  mixed valence species is stable with respect to conproportionation.

Similar observations were reported earlier in many binuclear systems [46,5c]. The value of  $K_{con}$  for complex **1** was found to be  $3.6 \times 10^5$  compared to the value of  $K_{con}$  ( $4.9 \times 10^6$ ) for complex **2** which confirms that complex **1** is more stable.

### 3.7. Quantum computational density functional theory based geometry optimization and molecular orbital analysis

The B3LYP/LAN2DZ level of theory was used to calculate bond angles and bond lengths. The selected bond lengths and angles are given along with the crystal data (Table 2). The quantum computational DFT calculated bond lengths and angles are similar to that of experimentally observed data. The calculated bond lengths and angles are slightly larger than the experimental (XRD) values since the quantum computational DFT calculation were performed on isolated molecules in the gas phase, whereas the XRD results were obtained in solid state[47]. The six important  $\alpha$  and  $\beta$  molecular orbitals (MO's) were analyzed for complexes **1** and **2**. These MO's with energy level diagrams are shown in Fig. 7 and 8. MO's play important roles in the electrical, optical and chemical reactions [48]. As these MO's can decide the way in which a molecule interacts with other chemical species, therefore,

these are known as the frontier molecular orbitals(MO's). These MO's may be highest occupied molecular orbitals (HO MO's) and lowest unoccupied orbitals (LUMO) and are important parameters for illustrating the chemical behavior (Fig. 7) of these molecular species[49]. The derived energy of six  $\alpha$  spin states (HOMO-2 to LUMO+2) for complex **1** are -6.538,-6.461,-5.461,-2.262,-0.950 and -0.818 eV respectively and energy gaps ( $\Delta E$ ) between HOMO-LUMO, HOMO-1-LUMO+1 and HOMO-2-LUMO+2 are 3.199,5.51 and 5.721eV, respectively. Similarly, six MO energies of the  $\beta$  spin state have been calculated. HOMO-2 to LUMO+2) are also calculated along with energy gaps as shown in Fig. 7. MO energies and the energy gaps were calculated for complex **2** as well and are depicted in Fig. 7. The energy gap in complex **1** is found to be larger than for complex **2**. The energy gap between the HOMO and LUMO orbitals indicate molecular chemical stability [18a]. A large HOMO-LUMO gap suggests a stable molecule with low chemical stability [18b]. Also, the energy gaps between the HOMO-LUMO orbitals are important parameters to decide the electrical transport properties of molecules [50]. Therefore complex **2** is more active than **1**.

The unpaired electrons remain in the HOMO and hence the HOMO are also known as singly occupied orbitals (SO MO's). In HOMO-LUMO structures of **1**, HOMO-1 and LUMO of  $\beta$  spins states are mainly constructed on the  $d_{x^2-y^2}$  magnetic orbital of the copper(II) atoms and  $sp^2$  hybrid orbitals of the oxygen atoms bearing the lone pairs in the bridging region. The exchange pathway is of the  $\sigma$  type. Moreover, SOMO's show that the atomic orbitals with a higher contribution to these HOMO's and LUMO's are those of the non-bridging atoms (oxygen and nitrogen atoms) of the Schiff base and the bridging moieties of the oxygen atoms in HOMO-2 and the  $\beta$  spins states. In **2**, the electron spin densities on non-bridging and bridging atoms are have a positive electron spin density (Fig. 8). In **2**, HOMO and LUMO+1 also showed electron spin density in the C = C moiety of the Schiff base (Fig. 8). This type of electron delocalization from copper centers to donor atoms is in agreement with the molecular structures obtained from single crystal X-ray analysis.

The molecular orbital analysis is used to predict the delocalization of electron density between occupied Lewis type natural molecular orbitals (NBO's), which correlate to stability donor acceptor (D-A) interactions[55]. As per molecular orbital analysis, all kind of interactions between the copper(II) atoms and coordinating atoms are referred to as coordinate bonds of the type  $N \rightarrow Cu$  or  $O \rightarrow Cu$ . Such types of D-A mechanisms are shown in Fig. 9. In such interactions electron density is transferred from the lone pair orbitals on the nitrogen or oxygen atoms, LP(N) or LP(O) to the antibonding LP\* (Cu). SOMO selected orbitals showing LP (N)  $\rightarrow$  LP\* (Cu) and LP (O)  $\rightarrow$  LP\* (Cu) interactions are shown in Fig. 9.

The spin density distribution was observed using the quantum computational DFT using the B3LYP/LANL2DZ basis set for the present complexes. The spin density is mainly delocalized into the copper(II) atom and those atoms which are bonded to copper(II) atom[5c]. The spin density of complexes is given as an example in Fig. 10. The positive sign of the densities are spread over the copper(II) atom and the negative sign of the densities were distributed over the donor atoms. These distributions were also supported with the HOMO-LUMO shapes observed in these copper(II) complexes.

### 3.8. Antioxidant superoxide dismutase (SOD) assay

The antioxidant SOD mimetic activities of these complexes has been evaluated and discussed. The antioxidant SOD activities of the complexes were evaluated by an NBT assay[52] following the reduction of NBT to MF<sup>+</sup> kinetically at 560 nm. These complexes exhibit significant catalytic activity toward the dismutation of superoxide anions. The concentration to attain 50% inhibition of the NBT reduction defined as IC<sub>50</sub> were estimated for complexes **1** and **2**(Table 6). The observed IC<sub>50</sub> values of

the present complexes were compared with earlier SOD mimics that have been reported[1f, 5c, 53, 54] (Table 6) and the value for the native SOD is also given for the comparison. The  $IC_{50}$  value for complex **2** (24  $\mu\text{mol}$ ) is less than **1** (35  $\mu\text{mol}$ ), thus, complex **2** is more antioxidant SOD active than **1**. The difference in  $IC_{50}$  value between **1** and **2** may be ascribed to structural variation, thus favouring ligand exchange and interaction with the substrate. The frontier molecular orbitals suffer a sustained change in coordination atmosphere around the metal centres in complex **2**. In complex **2**, Cu1 is six coordinate and Cu2 is five coordinate. Water molecules also play an important role for enhancing antioxidant SOD activity by guiding the  $O_2^{\cdot-}$  ion to enter and allow  $H_2O_2$  to leave rapidly from the copper centre. The same trend of biological activity is also verified from the quantum computational DFT calculations. The catalytic rate constant ( $k_{MCCF}$ ) was also evaluated for these complexes. The kinetic catalytic constant  $k_{MCCF}$  was obtained by the equation  $k_{MCCF} = k_{NBT} \times [NBT] / IC_{50}$ , where  $k_{NBT} = 5.94 \times 10^{-4} (\text{mol L}^{-1})^{-1} \text{s}^{-1}$  is the second order rate constant for NBT[55]. The kinetic catalytic constant ( $k_{MCCF}$ ) of **1** and **2** are  $9.50 \times 10^{-4} (\text{mol L}^{-1})^{-1} \text{s}^{-1}$  and  $13.84 \times 10^{-4} (\text{mol L}^{-1})^{-1} \text{s}^{-1}$ , respectively. The values of catalytic rate constants for the superoxide disproportionation constant ( $k_{MCCF}$ ) clearly indicate that the present complexes can be used as an antioxidant superoxide scavenger. Comparisons of  $k_{MCCF}$  for complexes **1** and **2** reveal that the geometry around copper contributes to the modulation of antioxidant SOD activity, with **2** being the best suited to react with superoxide free radicals. On the basis of antioxidant results, it is clear that complexes **1** and **2** are more efficient antioxidant than vitamin c, which is the standard for antioxidant superoxide dismutase[56].

### 3.9. Structure activity relationship

The catalytic role of the stable sulfate/succinato bridge can be well understood according to a mechanism suggested in the literature[57] (Scheme 6). The dismutation of  $O_2^{\cdot-}$  may take place in the following steps: First,  $O_2^{\cdot-}$  displaces an  $H_2O$  molecule and binds directly to a copper(II) ion and gives up its electron. Second, the  $O_2^{\cdot-}$  binding directly to the copper(II) ion can be exchanged rapidly between the axial and the planar position of the distorted square pyramid, leading it to give up its electron and form an  $O_2$  molecule. Third, the sulfate/succinato bridge breaks and the electrically neutral oxygen molecule leaves. The O atom of sulfate/succinato bridge gets its proton from the bulk solvent and copper(II) reduces to copper(I) [Scheme 6 (iv)]. Fourth, a second  $O_2^{\cdot-}$  binds again to the copper(I) ion and accepts an electron. Since the proton exchange between the substrates and buffer is a rapid process,

the  $O_2^{\cdot-}$  further combines with another proton from the solution to form an  $H_2O_2$  molecule. Finally, the sulfate/succinato bridge re-forms and electrically neutral  $H_2O_2$  leaves from the system, completing a catalytic cycle.

The reduction potentials of the present complexes are compared with the bovine and human SOD metalloenzyme[55c]. Fortunately, reduction potentials of complexes **1** and **2** are lower than the reduction potential values of 0.115 and 0.075V/SHE for the bovine and human SOD respectively, but in a very good range for promoting dismutation of the  $O_2^{\cdot-}$  anion as shown by the high catalytic activity. High SOD activity observed for complexes **1** and **2** could be explained in terms of fast exchange of axial water molecules and less steric hindrance to the  $O_2^{\cdot-}$  moiety in these complexes. These complexes have potent SOD activity and may be considered as therapeutic agents with a small molecular weight compared to native SOD. Furthermore, the moderately high SOD activities of complexes **1** and **2** may also be related to possible cooperation of two copper(II) centres, in close proximity, in free radical binding and electron transfer through the sulfate/succinato bridge. In native SOD, one Cu(II) may resemble the role of a mimic through the imidazolato bridge, in controlling the electron density of the redox action copper center[55d]. The relatively high SOD activity of complex **2** could be due to some structural variation.

#### 4. Conclusions

A dual approach comprising the experimental and quantum computational study of two new bridged binuclear copper(II) coordination complexes **1** and **2** that have been synthesized by metal *N'*-[(*E*)-pyridin-2-ylmethylidene] benzohydrazide appear to be good models for superoxide dismutase. For complexes **1** and **2**, we were able to appropriately fit magnetic susceptibility data. Complex **1** has bridging sulfate and two oxygen atoms of two O, N, N' ligands. Complex **2** has bridging succinate and also two oxygen atoms of two same ligands. The extensive ligand based hydrogen bonding,  $CH \cdots \pi$ ,  $\pi \cdots \pi$  and  $lp \cdots \pi$  (metal chelate) interactions in both complexes have resulted into new intriguing 3-D supramolecular structures. The cryomagnetic susceptibility data revealed that the copper(II) centers in **1** and **2** are antiferromagnetically coupled ( $J = -1.50$ )  $cm^{-1}$  for **1** and ( $J = -7.7$ )  $cm^{-1}$  for **2**). Electrochemical studies of binuclear complexes **1** and **2** showed two redox waves. Coordinated water molecules in both complexes create well directed H-bonding activity. Bond lengths and angles from computational DFT calculations have been compared with those obtained from single X-ray techniques

and agreements between them have been observed. In addition, antioxidant (SOD) measurements indicate that both complexes behave as superoxide dismutase bio mimetic systems. In both complexes coordination sites available for the binding of  $O_2^{\cdot-}$  as shown by the X-ray structures show antioxidant SOD activity.

### **Acknowledgements**

Authors thanks RSIC (SAIF) IIT, Bombay for EPR measurements SAIF, Central Drug Research Institute, Lucknow, are thankfully acknowledged for providing analytical, spectral facilities. Authors acknowledge Dr. Alok Banerjee, UGC-DAE CSR, Indore, for providing the low temperature magnetic measurement facility. The authors wish to acknowledge the assistance of Dr. Matthias Zeller in the collection of diffraction data and NSF Grant CHE 0087210, Ohio Board of Regents Grant CAP-491, and by Youngstown State University for funds to purchase the X-ray diffractometer.

## References

- [1] (a) S.K. Shakhathreh, E.G. Bakalbassis, I. Brudgam, H. Hartl, J.Mrozinski and C.A. Tsipis, *Inorg.Chem.* 30 (1991) 2801; (b) R. Karmakar, C.R. Choudhury, D.L. Hughes, G.P.A. Yap, M.S. El Fallah, C. Desplanches, J.-P. Sutter, S. Mitra, *Inorg. Chim. Acta* 359 (2006) 1184; (c) C. Adhikary, D. Mal, K.I. Okamoto, S. Chaudhury, S. Koner, *Polyhedron* 25 (2006) 2191; (d) S. Banerjee, M.G.B. Drew, C.-Z. Lu, J. Tercero, A. Ghosh, *Eur. J. Inorg. Chem.* (2005) 2376; (e) A. Ray, S. Banerjee, R.J. Butcher, C. Desplanches and S. Mitra, *Polyhedron* 27 (2008) 2409; (f) R.N. Patel, D.K. Patel, V.P. Sondhiya, K.K. Shukla, Y. Singh and A. Kumar, *Inorg. Chim. Acta* 405 (2013) 209.
- [2] (a) R. Glier, M. Jorand, C. Waegell and B.J. Chem. Soc., *Chem. Commun.* (1990) 1752; (b) K.D. Karlin, Z. Tyeklar. *Bioinorganic Chemistry of Copper*, Chapman and Hall, New York (1993); (c) B. Reinhammer, *Copper Proteins and Copper Enzymes*, Vol. 3, 1, CRC Press, Boca Raton, FL (1984); (d) K.A. Magnus, H. Ton-That and J.E. Carpenter, *Chem. Rev.* 94 (1994) 727; (e) E.I. Solomon, U.M. Sundaram and T.E. Mackonkin. *Chem. Rev.* 96 (1996) 2563; (f) N. Kitajima and Y. Moro-oka. *Chem. Rev.* 94 (1994) 737; (g) S. Ryan, H. Adams, D.E. Fenton, M. Becker and S. Schindler. *Inorg. Chem.* 37 (1998) 2134; (h) P.L. Holland and W.B. Tolman. *Coord. Chem. Rev.* 55 (1999) 190; (i) H. Decker, R. Dillinger and F. Tuczek. *Angew. Chem. Int. Ed.* 39 (2000) 1591; (j) C. Gerdemann, C. Eicken and B. Krebs. *Acc. Chem. Res.* 35 (2002) 183; (k) G. Dutta, R.K. Debnath, A. Kalita, P. Kumar, M. Sarma, R. Boomi. Shankar and B. Mondal, *Polyhedron* 30 (2011) 293.
- [3] S. J. Lippard "Bioinorganic Chemistry: A Maturing Frontier." *Science* 261 (1993) 699.
- [4] A.E.G. Cass, *Superoxide Dismutases in Metalloproteins*, ed. P.M. Harrison, Verlag Chemie, Basel, Ch. 4, 1 (1985) 121.
- [5] (a) R.N. Patel, A. Singh, K.K. Shukla, Dinesh K. Patel V.P. Sondhiya, Y. Singh and R. Pandey, *J. Coord. Chem.* 65 (2012) 1381; (b) R. N. Patel, V. P. Sondhiya, K.K. Shukla, D.K. Patel and Y. Singh, *Polyhedron* 50 (2013) 139; (c) R. N. Patel, Y. Singh, Y.P. Singh, A.K. Patel, N. Patel, R. Singh, R.J. Butcher, J.P. Jasinski, E. Colacio and M.A. Palacios, *New J. Chem.* 42 (2018) 3112.
- [6] (a) R.N. Patel, S. Rawat, M. Choudhary, V.P. Sondhiya, Dharendra K. Patel, K.K. Shukla, Dinesh K. Patel, Y. Singh and R. Pandey *Inorg. Chim. Acta* 392 (2012) 283; (b) R. N. Patel, Y. Singh, Y.P. Singh, R.J. Butcher, Arti Kamal, I.P. Tripathi, *Polyhedron* 117 (2016) 20; (c) R.N. Patel, Y.P. Singh, Y. Singh, R.J. Butcher, Jerry P. Jasinski, *Polyhedron* 129 (2017) 164.

- [7] (a) N.R. Sangeetha and S. Pal, *Polyhedron* 19 (2000) 1593; (b) S. Banerjee, S. Sen, S. Basak, S. Mitra, D. Hughes and C. Desplanches *Inorg. Chim. Acta* 361 (2008) 2707; (c) R.N. Patel, D.K. Patel, K.K. Shukla, and Y. Singh, *J. Coord. Chem.* 66 (2013) 4131.
- [8] (a) Y.Q. Zheng, J.L. Lin, *Z. Kristallogr. NCS* 215 (2000) 157; (b) M. Fleck, E. Tillmanns, L. Bohaty, *Z. Kristallogr. NCS* 215 (2000) 429; (c) M. Padmanabhan, S.M. Kumary, X. Huang, J. Li, *Inorg. Chim. Acta* 358 (2005) 3537.
- [9] (a) M.L. Calatayud, I. Castro, J. Sletten, F. Lloret, M Julve, *Inorg. Chim. Acta* 300-302 (2000) 846; (b) A. Bacchi, M. Carcelli, G. Pelizzi, C. Solinas, L. Sorace, *Inorg. Chim. Acta* 359 (2006) 2275; (c) J.R. Zimmerman, A. de B.-Dias, *Inorg. Chem. Commu.* 14 (2011) 753; (d) G. Mezei, *Acta Cryst. E* 72 (2016) 1064.
- [10] (a) J.W. Steed, D.R. Turner and K.J. Wallace, *Core Concepts in Supramolecular Chemistry and Nanochemistry*, John Wiley and Sons, Weinheim (2007); (b) P.W.N.M. Leeuwen, *Supramolecular Catalysis*, John Wiley & Sons, Weinheim (2008); (c) K.Y. Choi and K.J. Kim, *Polyhedron* 27 (2008) 1310.
- [11] D.D. Perrin, W.L.F. Armario and D.R. Perrin, *Purification of laboratory Chemicals*, 2<sup>nd</sup> Ed., Pergamon: Oxford, England (1980).
- [12] G. M. Sheldrick, *Acta Cryst. A* 71 (2015) 3.
- [13] G. M. Sheldrick, *Acta Cryst. C* 71 (2015) 3.
- [14] Gaussian 09, Revision D.01, M.J. Frisch, G.W. Trucks, H.B. Schlegel, G.E. Scuseria, M.A. Robb, J.R. Cheeseman, G. Scalmani, V. Barone, B. Mennucci, G.A. Petersson, H. Nakatsuji, M. Caricato, X. Li, H. P. Hratchian, A. F. Izmaylov, J. Bloino, G. Zheng, J.L. Sonnenberg, M. Hada, M. Ehara, K. Toyota, R. Fukuda, J. Hasegawa, M. Ishida, T. Nakajima, Y. Honda, O. Kitao, H. Nakai, T. Vreven, J.A. Montgomery, Jr., J.E. Peralta, F. Ogliaro, M. Bearpark, J. J. Heyd, E. Brothers, K.N. Kudin, V.N. Staroverov, T. Keith, R. Kobayashi, J. Normand, K. Raghavachari, A. Rendell, J.C. Burant, S.S. Iyengar, J. Tomasi, M. Cossi, N. Rega, J.M. Millam, M. Klene, J. E. Knox, J.B. Cross, V. Bakken, C. Adamo, J. Jaramillo, R. Gomperts, R. E. Stratmann, O. Yazyev, A.J. Austin, R. Cammi, C. Pomelli, J.W. Ochterski, R.L. Martin, K. Morokuma, V. G. Zakrzewski, G.A. Voth, P. Salvador, J.J. Dannenberg, S. Dapprich, A.D. Daniels, O. Farkas, J.B. Foresman, J.V. Ortiz, J. Cioslowski, and D.J. Fox, Gaussian, Inc., Wallingford CT (2013).
- [15] Gauss View 5.0.9(Gaussian Inc., Wallingford, CT, USA (2009).
- [16] A.E. Reed, R.B. Weinstock and F. Weinhold, *J. Phys.Chem.* 83 (1985) 735.
- [17] (a) R. Bauernschmitt and R. Ahlrichs, *Chem. Phys. Lett.* 256 (1996) 454; (b) R.E. Stratmann, G.E. Scuseria and M.J. Frisch, *J. Chem. Phys.* 109 (1998) 8218; (c) M.E. Casida, C. Jamorski, K.C. Casida and D.R. Salahub, *J. Chem. Phys.* 108 (1998) 4439.

- [18] (a) V. Barone and M. Cossi, *J. Phys. Chem. A* 102 (1998) 1995; (b) M. Cossi and V. Barone, *J. Chem. Phys.* 115 (2001) 4708.
- [19] R.G. Bhirud and T.S. Shrivastava, *Inorg. Chim. Acta* 173 (1990) 121.
- [20] (a) Y. Singh, R. N. Patel, Y.P. Singh, A.K. Patel, N. Patel, R. Singh, R.J. Butcher, J.P. Jasinski, E. Colacio and M.A. Palacios, *Dalton Trans.* 46 (2017) 11860; (b) R.N. Patel, N. Singh, K.K. Shukla, V.L.N. Gundla and U.K. Chauhan *J. Inorg. Biochem.* 992 (2005) 651.
- [21] (a) A. Datta, S.C. Sheu, P.H. Liu and J.H. Huang. *Acta Cryst. Sec. 67 E* (2011) m1852; (b) T.E. Khalil, L. Labib and M.F. Iskander, *Polyhedron* 13 (1994) 2569; (c) R.N. Patel, Y. Singh, Y.P. Singh and R.J. Butcher, *J. Coord. Chem.* 69 (2016) 2377.
- [22] M.E. Reichmann, S.A. Rice, C.A. Thomas and P. Doty, *J. Am. Chem. Soc.* 76 (1954) 3047.
- [23] K. Nakamoto, *Infrared and Raman Spectra of Inorganic and Coordination Compounds*, Wiley, New York (1986) .
- [24] (a) L. El-Sayed and M.F. Iskander, *J. Inorg. Nucl. Chem.* 33 (1971) 435; (b) S. Choudhury, M. Kakoti, A.K. Deb and S. Goswami, *Polyhedron* 11 (1992) 3183.
- [25] (a) W.J. Geary. *Coord. Chem. Rev.* 7 (1971) 81; (b) R.N. Patel, A. Singh, K.K. Shukla, D.K. Patel and V.P. Sondhiya, *Trans. Met. Chem.* 36 (2011) 179.
- [26] N. Baralde, W.E. Nacif, L.R. Teixeira and T.S. Reboucas, *Trans. Met. Chem* 27 (2002) 85.
- [27] (a) A.W. Addison, T.N. Rao, J. Reedijk, J. Van Rijn and C.G. Verschoor, *J. Chem. Soc. Dalton Trans.* (1984) 1349; (b) K.D. Karlin, J.C. Hayes, S. Juen, J.P. Hutchinson and J. Zubieta, *Inorg. Chem.* 21 (1982) 4106.
- [28] E. Gungor, H. Kara, E. Colacio and A.J. Mota, *Eur. J. Inorg. Chem.* 2014 (2014) 1552.
- [29] (a) M. Drillon, A. Grand and P. Rey, *Inorg. Chem.* 29 (1990) 771; (b) G.A. van Albada, M.T. Lakin, N. Veldman, A.L. Spek, and J. Reedijk, *Inorg. Chem.* 34 (1995) 4910.
- [30] M.C. Hu, Y. Wang, Q.G. Zhai, S.N. Li, Y. Jiang and C. Zhang, *Inorg. Chem.* 48 (2009) 1449.
- [31] H. Masui, *Coord. Chem. Rev.* 957 (2001) 219.
- [32] (a) S. Sarkhel, A. Rich and M. Egli, *J. Am. Chem. Soc.* 125 (2003) 8998 ;( b) M. Egli and S. Sarkhel, *Acc Chem Res* 40 (2007)197; (c) T.J. Mooibroek, P. Gamez and J. Reedijk, *Cryst. Eng. Comm.* 10 (2008) 1501.
- [33] M. Raimondi, G. Calderoni, A. Famulari, L. Raimondi and F. Cozzi, *J. Phys. Chem. A* 107 (2003) 772.
- [34] B. Bleaney and K.D. Bowers, *Proc. R. Soc. London, A* 214 (1952) 451.

- [35] O. Kahn, *Molecular Magnetism*, VCH, New York (1993).
- [36] (a) B.J. Hathaway and D.E. Billing, *Coord. Chem. Rev.* 5 (1970) 143; (b) A.B.P. Lever, *Inorganic Electronic Spectroscopy*, 2<sup>nd</sup> ed.; Elsevier: New York (1984).
- [37] (a) H. Ohtsu, Y. Shimazaki, A. Odani, O. Yamauchi, W. Mori, S. Itoh and S. Fukuzum, *J. Am. Chem. Soc.* 122 (2000) 5733; (b) S. Mukhopadhyay, D. Mandal, P.B. Chatterjee, C. Desplanches, J.P. Sutter, R.J. Butcher and M. Chaudhury, *Inorg. Chem.* 43 (2004) 8501.
- [38] R. Cao, Q. Sun, D. Sun, M. Hong, W. Bi and Y. Zhao, *Inorg. Chem.* 41 (2002) 6161; (b) T.M. Donlevy, L.R. Gahan, T.W. Hambley, G.R. Hanson, K.L. McMahon and R. Stranger, *Inorg. Chem.* 33 (1994) 5131.
- [39] N.D. Chasteen and R.L. Belford, *Inorg. Chem.* 9 (1970) 169.
- [40] (a) W. E. Estes, J. W. Wasson, W. E. Hall and W. E. Hatfield, *Inorg. Chem.* 17(1978) 3657; (b) R. C. Aggarwal, N. K. Singh and R. P Singh, *Inorg. Chem.* 20(1981) 2794; (c) W. A. Alves, S. A. Almeida-Folho, R. H. A Santos and A. M. D. C. Ferreira, *Inorg. Chem. Commun.* 6(2003) 294;(d) O. Kahn, *Molecular Magnetism*, Wiley VCH, New York, 1993
- [41] a) S. K. Jain, B. S. Garg, Y. K. Bhoon, D. L. Klayman and J. P. Scovill, *Spectrochim. Acta, Part A*, 41(1985)407; (b) M. J. Bew, B. J. Hathaway and R. J. Faraday, *J. Chem. Soc., Dalton Trans.*, 1972, 1229.
- [42] B.A. Goodman, R.D. Johnston, E.M. Larsen, J.F. Nixon, J.B. Raynor, *Advances in inorganic chemistry and radiochemistry* 13(1970) Academic Press, New York and London.
- [43] E. Garibba and G. Micera, *J. Chem. Educ.* 83(2006) 1229.
- [44] Zanello, *Inorganic Electrochemistry: Theory, Practice and Applications*; The Royal society of Chemistry, U. K. (2003) 110.
- [45] (a) W. Zhang, S. Liu, C. Ma and D. Jiang, *Polyhedron* 17 (1998) 3835; (b) U. Ranjedran, R. Viswanathan, M. Palaniandavar and M. Lakshminarayanan, *J. Chem. Soc., Dalton Trans.* (1992) 3563.
- [46] C. Bethe, C. Beguin, I.G. Luneau, S. Hamman, C. Philouze, J.L. Pierre, F. Thomas and S. Torrelli, *Inorg. Chem.* 41 (2002) 479.
- [47] (a) S.K. Patel, R.N. Patel, Y. Singh, Y.P. Singh, D. Kumhar, R.N. Jadeja, H. Roy, A.K. Patel, N. Patel, N. Patel, A. Banerjee, D. C. -Lazarte and A. Gutierrez, *Polyhedron* 161 (2019) 198; (b) F. Zhang, Y. Tang, Z. Cao, W. Jing, Z. Wu and Y. Chen, *Corros. Sci.* 61 (2012) 1.
- [48] (a) R.R. Gagne, C.A. Koval and T.J. Smith, *J. Am. Chem. Soc.* 99 (1977) 8367; (b) R.R. Gagne, J.L. Allison, R.S. Gall and C. A. Koval, *J. Am. Chem. Soc.* 99 (1977) 7170; (c) R.R. Gagne, C.A. Koval, T.J. Smith and M.C. Cimolino, *J. Am. Chem. Soc.* 101 (1979) 4571; (d) F. Ammar and J.M. Saveant, *J. Electronal. Chem.* 47 (1973) 115; (e) C. Creutz, *J. Am. Chem. Soc.* 95 (1973) 1086; (f) W.H. Morrison, S. Krogsrud and D.N. Hendrickson, *Inorg. Chem.* 12 (1973) 1998.
- [49] I. Fleming, *In frontier molecular orbitals and Organic chemical reactions*, London, Willy (1976).
- [50] D. Shobaa, S. Periandy, M. Karabacak, S. Ramalingam, *Spectrochim. Acta*, 83 (2011) 540.

- [51] R.K. Dennington, T. Millam, in: S.M. KS (Ed.), *J. Semichem. Inc* (2009).
- [52] R.N. Patel, N. Singh, K.K. Shukla, U.K. Chauhan, S. Chakraborty, J. Niclos-Gutierrez and A. Castineiras, *J. Inorg. Biochem.* 98 (2004) 231.
- [53] (a) R.N. Patel, *Inorg. Chim. Acta* 363 (2010) 3838; (b) R.N. Patel, Y.P. Singh, Y. Singh, R.J. Butcher, M. Zeller, R.K.B. Singh, OU. Wang, *J. Mole. Struct.* 1136 (2017) 157; (c) R.N. Patel, N. Singh, K.K. Shukla, V.L.N. Gundla and U.K. Chauhan, *J. Inorg. Biochem.* 99 (2005) 651; (d) A. Mederos, R. Diaz, A.M. Villalonga and R. Cao, *J. Coord. Chem.* 62 (2009) 100; (e) Y. P. Singh, R.N. Patel, Y. Singh, R.J. Butcher, P.K. Vishakarma, R.K. Bhubon Singh, *Polyhedron* 122 (2017) 1; (f) U. Weser, L.M. Schubotz and E. Lengfelder *J. Mol. Catal.* 13 (1981) 249; (g) G. Tabbi, W.L. Driessen, J. Reedijk, R. P. Bonomo and N. Veldman, *Inorg. Chem.* 36 (1997) 1168; (h) J.L. Pierre, P. Chautemps, S. Refaif, C. Beguin, A.E. Marzouki, G. Serratrice, E. Saint-Aman and P. Rey, *J. Am. Chem. Soc.* 117 (1995) 1965.
- [54] (a) P.J. Hart, M.M. Balbirnie, N.L. Ogigara, A.M. Nersissian, M.S. Weiss, J.S. Valentine and D. Eisenberg, *Biochemistry* 38 (1999) 2167; (b) Y.P. Singh, R.N. Patel, Y. Singh, Duane C. -Lazarte and R.J. Butcher, *Dalton Trans.* 46 (2017) 2803; (c) R.N. Patel, Y.P. Singh, Y. Singh, R.J. Butcher and M. Zeller, *RSC Adv.* 6 (2016) 107379; (e) I. Bertine, L. Banci, M. Piccioli and C. Luchinat, *Coord. Chem. Rev.* 100 (1990) 67.
- [55] (a) S. Durot, C. Policar, F. Cisnetti, F. Lambert, J.P. Renault, G. Pelosi, G. Blain, H. Korri-Youssoufi and J.P. Mahy, *Eur. J. Inorg. Chem.* (2005) 3513; (b) T. Yoshida, T. Matsuda, T. Okano, T. Kitani and S. Otsuka, *J. Am. Chem. Soc.* 101 (1979) 2027; (c) L. M. Ellerby, D. E. Cabelli, J. A. Graden and J. S. Valentine, *J. Am. Chem. Soc.* 118 (1996) 6556; (d) P. Starha, ZdekTrávníček, R. Herchel, I. Popa, P. Suchy and J. Vanco, *J. Inorg. Biochem.* 103 (2009) 432.
- [56] (a) Y. Li, Z.-Y. Yang and J.-C. Wu, *European Journal of Medicinal Chemistry* 45 (2010) 5692; (b) R. Xing, H. Yu, S. Liu, W. Zhang, Q. Zhang, Z. Li and P. Li, *Bioorganic & Medicinal Chemistry* 13 (2005) 1387.
- [57] T. Fukai, M. U. -Fukai, *Antioxid. Redox Signal* 15 (2011) 1583.

Fig. 1. (a) Molecular structure of **1** showing the atom labelling scheme of the asymmetric unit, (b) Coordination sphere of **1**, (c) Hydrogen bonding, weak intermolecular interactions and heterosynthon graph-set ring motifs for **1** (blue dashed lines), (d) Weak CH $\cdots\pi$  and H $\cdots\pi$  intermolecular interactions (dashed lines) for **1**, (dashed lines), (e) Weak  $\pi\cdots\pi$  stacking inter- and intramolecular interactions for **1** (dashed lines), (f) Uncoordinated solvent molecules along with lone pair interactions for **1** (dashed lines)

Fig. 2. (a) Molecular structure of **2** showing the atom labelling scheme of the asymmetric unit, (b) Coordination sphere of **2**, (c) Hydrogen bonding, weak intermolecular interactions and heterosynthon graph-set ring motifs for **2** (blue dashed lines), (d) Weak CH $\cdots\pi$  and H $\cdots\pi$  intermolecular interactions (dashed lines) for **2**, (dashed lines), (e) Weak  $\pi\cdots\pi$  stacking inter- and intramolecular interactions for **2**, (dashed lines), (f) Uncoordinated perchlorate ion along with lone pair interactions for **2**, (dashed lines)

Fig. 3. Temperature dependence of  $\chi T$  and  $\chi$  (inset) for complex **1**. The solid line represents the fit using the equation and parameters described in the text

Fig. 4. Temperature dependence of  $\chi T$  and  $\chi$  (inset) for complex **2**. The solid line represents the fit using the equation and parameters described in the text

Fig. 5. (a) EPR spectra of complex **1** in polycrystalline state (RT) and DMSO solution at liquid nitrogen temperature (LNT), inset half-field at RT and LNT. (b) EPR spectra of complex **2** in the polycrystalline state (RT) and in DMSO solution at liquid nitrogen temperature (LNT), inset half-field at RT and LNT

Fig. 6. (a) Cyclic voltammograms for **1** and **2** in DMSO at an Ag/AgCl electrode with scan rate 100 mV s $^{-1}$  and temperature 25  $^{\circ}$ C. (b) Differential pulse voltammogram (DPV) for **1** and **2** at room temperature using a scan rate 20 mV s $^{-1}$  in DMSO. The pulse amplitude is 50 mV

Fig. 7. HOMO-LUMO structure with energy level diagram for complex **1**

Fig. 8. HOMO-LUMO structure with energy level diagrams for complex **2**

Fig. 9. The donor and acceptor orbitals involved in the donor-acceptor (D-A) mechanism interactions in complexes **1** and **2**

Fig. 10. (a) Spin density of complex **1**; (b) Spin density of complex **2**

Scheme 1. Half reactions for the dismutation of the superoxide radical mediated by the Cu-SOD enzyme.

Scheme 2. Synthesis of complexes **1** and **2** is based on the active site structure of Cu-Zn SOD. (A) The structure of Cu-Zn SOD. (B) Structures of complexes **1** and **2**.

Scheme 3. Condensation of salicylhydrazide with 2-pyridine carboxylaldehyde which subsequently leads to the formation of N'-[(E)-pyridin-2-ylmethylidene]benzohydrazide

Scheme 4. Synthetic routes of complexes **1** and **2**

Scheme 5. Schematic representations of the orientations of *d* and *p* atomic orbitals for the metal and bridged moieties in complexes **1** and **2**

Scheme 6. Schematic diagram of the proposed  $\text{O}_2^-$  dismutation reaction catalyzed by **1** steering the  $\text{O}_2^-$  to  $\text{Cu}^{2+}$ .

Table 1. Crystal data and structure refinement parameters for the structures **1** and **2**

Complex	<b>1</b>	<b>2</b>
Empirical formula	$\text{C}_{26}\text{H}_{25}\text{Cu}_2\text{N}_6\text{O}_{8.50}\text{S}$	$\text{C}_{30}\text{H}_{28}\text{ClCu}_2\text{N}_6\text{O}_{11}$
Formula weight	716.66	811.11
Temperature	150(2) K	100(2) K
Wavelength	0.71073 Å	0.71073 Å
Crystal system	Triclinic	Triclinic

Space group	$P\bar{1}$	$P\bar{1}$
Unit cell dimensions Å, °		
a	9.6229(19)	9.882(4)
b	12.665(3)	12.373(5)
c	14.924(3)	15.488(6)
$\alpha$	69.20(3)	97.829(6)
$\beta$	73.93(3)	108.340(6)
$\gamma$	74.54(3)	106.769(6)°
Volume	1604.9(7) Å <sup>3</sup>	1666.5(11) Å <sup>3</sup>
Z	2	2
Density (calculated)	1.483 Mg/m <sup>3</sup>	1.616 Mg/m <sup>3</sup>
Absorption coefficient	1.446 mm <sup>-1</sup>	1.425 mm <sup>-1</sup>
F(000)	730	826
Crystal size	0.33 x 0.26 x 0.21 mm <sup>3</sup>	0.250 x 0.210 x 0.090 mm <sup>3</sup>
Theta range for data collection	2.933 to 25.252°	1.982 to 26.935°
Index ranges	-11<=h<=11, -14<=k<=15, -17<=l<=17	-12<=h<=12, -15<=k<=15, -19<=l<=19
Reflections collected	12405	21623
Independent reflections	5812 [R(int) = 0.2687]	7120 [R(int) = 0.0405]
Completeness to theta = 25.252°	99.8 %	99.3 %
Absorption correction	Semi-empirical from equivalents	Semi-empirical from equivalents
Max. and min. transmission	0.7509 and 0.6466	0.7455 and 0.6045
Refinement method	Full-matrix least-squares on F <sup>2</sup>	Full-matrix least-squares on F <sup>2</sup>
Data / restraints / parameters	5812 / 11 / 403	7120 / 53 / 477
Goodness-of-fit on F <sup>2</sup>	0.868	1.034
Final R indices [I>2sigma(I)]	R1 = 0.0950, wR2 = 0.2069	R1 = 0.0507, wR2 = 0.1472
R indices (all data)	R1 = 0.2209, wR2 = 0.2885	R1 = 0.0676, wR2 = 0.1592
Extinction coefficient	n/a	n/a
Largest diff. peak and hole	0.673 and -0.927 e.Å <sup>-3</sup>	1.880 and -0.708 e.Å <sup>-3</sup>

Table 2. Selected bond lengths and angles for structures **1** and **2** [Å and °].

Parameters	Single crystal XRD data	Theoretical data*	Parameters	Single crystal XRD data	Theoretical data*
<b>1</b>					
Bond lengths					
Cu(1)-O(1)	1.904(8)	2.1012	Cu(1)-N(2A)	1.936(9)	2.1214
Cu(1)-O(1A)	1.968(7)	2.1832	Cu(1)-N(1A)	2.027(9)	2.1912
Cu(2)-N(2B)	1.924(10)	2.1092	Cu(2)-O(2)	1.932(8)	2.1502
Cu(2)-N(1B)	1.978(8)	2.0919	Cu(2)-O(1B)	1.993(7)	2.1410
Cu(2)-O(1W)	2.293(8)	2.3320	Cu(2)-O(1A)	2.745(10)	2.849
Bond angles					
O(1)-Cu(1)-N(2A)	170.2(4)	173.4	O(1)-Cu(1)-O(1A)	99.0(3)	100.4
N(2A)-Cu(1)-O(1A)	80.2(3)	81.8	O(1)-Cu(1)-(1A)	99.9(4)	101.3
N(2A)-Cu(1)-N(1A)	80.5(4)	81.9	O(1A)-Cu(1)-(1A)	160.6(4)	161.8
N(2B)-Cu(2)-O(2)	171.5(3)	173.2	N(2B)-Cu(2)-(1B)	81.5(4)	82.7
O(2)-Cu(2)-N(1B)	97.2(4)	98.7	N(2B)-Cu(2)-(1B)	78.8(4)	79.9
O(2)-Cu(2)-O(1B)	101.1(3)	102.7	N(1B)-Cu(2)-(1B)	158.6(4)	159.8
N(2B)-Cu(2)-O(1W)	95.9(3)	97.0	O(2)-Cu(2)-(1W)	92.6(3)	93.7
N(1B)-Cu(2)-O(1W)	94.0(3)	95.6	O(1B)-Cu(2)-(1W)	96.2(3)	97.8
<b>2</b>					
Bond lengths					
Cu(1)-N(2A)	1.936(3)	2.0837	Cu(1)-O(1)	1.943(3)	2.1084
Cu(1)-O(1A)	1.994(3)	2.1385	Cu(1)-N(1A)	2.011(3)	2.1819
Cu(1)-O(1W)	2.284(3)	2.3397	Cu(1)-O(1A)	2.703(3)	2.8197
Cu(2)-O(2)	1.921(3)	2.1546	Cu(2)-N(2B)	1.922(3)	2.0978
Cu(2)-O(1B)	1.969(3)	2.1987	Cu(2)-N(1B)	2.008(3)	2.2280
Cu(2)-O(1A)	2.379(3)	2.4927			
Bond angles					
N(2A)-Cu(1)-O(1)	173.00(11)	174.8	N(2A)-Cu(1)-(1A)	78.87(12)	80.7
O(1)-Cu(1)-O(1A)	99.64(11)	100.7	N(2A)-Cu(1)-(1A)	80.47(13)	81.5

O(1)-Cu(1)-N(1A)	100.27(12)	101.3	O(1A)-Cu(1)-(1A)	158.75(12)	160.5
N(2A)-Cu(1)-O(1W)	97.27(11)	98.3	O(1)-Cu(1)-O(1W)	89.69(11)	91.1
O(1A)-Cu(1)-O(1W)	97.13(11)	99.2	N(1A)-Cu(1)-(1W)	90.35(12)	91.5
O(2)-Cu(2)-N(2B)	174.18(12)	175.2	O(2)-Cu(2)-O(1B)	102.18(11)	103.0
N(2B)-Cu(2)-O(1B)	79.63(12)	80.9	O(2)-Cu(2)-N(1B)	96.81(12)	98.3
N(2B)-Cu(2)-N(1B)	80.92(13)	81.9	O(1B)-Cu(2)-(1B)	160.17(12)	161.8
O(2)-Cu(2)-O(1A)	88.10(11)	90.0	N(2B)-Cu(2)-(1A)	97.48(11)	98.3
O(1B)-Cu(2)-O(1A)	88.93(10)	90.1	N(1B)-Cu(2)-(1A)	97.43(11)	98.2

\*TD-DFT/B3LYP/LANL2DZ Calculations

Table 3. Hydrogen bond lengths and angles for structures 1 and 2 [ $\text{\AA}$  and  $^\circ$ ].

D-H...A	d(D-H)	d(H...A)	d(D...A)	$\angle(\text{DHA})$	Symmetry transformations used to generate equivalent atoms:
<b>1</b>					
O(1W)-H(1W1)...N(3B)#1	0.812(15)	2.07(2)	2.881(13)	176(3)	#1 -x+1
O(2W)-H(2W2)...O(1W)	0.82(2)	2.12(7)	2.787(12)	139(10)	-y+1
O(3W)-H(3W1)...O(1)	0.81(2)	2.45(8)	3.055(16)	132(9)	-z+1
C(6A)-H(6AA)...O(1W)#2	0.95	2.62	3.454(14)	146.0	#2 x+1 y,z
C(2B)-H(2BA)...O(1A)#3	0.95	2.44	3.384(17)	173.1	#3 -x+1 -y
C(6B)-H(6BA)...O(2W)#1	0.95	2.65	3.59(2)	171.6	-z+1
<b>2</b>					
O(1W)-H(1W1)...Cl(1)	0.835(18)	2.914(19)	3.741(4)	171(4)	#1 -x+1,
O(1W)-H(1W1)...O(12)	0.835(18)	1.98(2)	2.782(6)	161(3)	-y+1
O(1W)-H(1W1)...O(14A)	0.835(18)	2.29(4)	3.05(2)	152(3)	-z+1 #2
O(1W)-H(1W2)...N(3A)#1	0.817(18)	2.02(2)	2.818(4)	164(4)	-x+2
C(3)-H(3A)...O(14)#2	0.99	2.40	3.276(6)	146.7	-y+1
C(3)-H(3A)...O(11A)#2	0.99	2.29	3.267(19)	167.8	-z+2 #3
C(2A)-H(2AA)...O(1B)#3	0.95	2.57	3.494(5)	164.3	-x+1-y
C(6A)-H(6AA)...O(12)#1	0.95	2.45	3.392(7)	169.6	-z+1#4
C(6A)-H(6AA)...O(14A)#1	0.95	2.26	3.18(3)	162.4	-x+1
C(1B)-H(1BA)...O(4)	0.95	2.62	3.345(6)	133.4	-y+1
C(2B)-H(2BA)...O(13)#4	0.95	2.62	3.276(6)	127.0	-z+2

Table 4. EPR parameters of copper(II) complexes 1 and 2.

EPR parameter	1	2
<i>Polycrystalline state (298 K)</i>		
$g_{\parallel}$	2.237	2.171
$g_{\perp}$	2.060	2.060
G	3.410	2.924
D ( $\text{cm}^{-1}$ )	0.090	0.095
<i>Frozen solution in DMSO (77 K)</i>		
$g_{\parallel}$	2.200	2.218
$g_{\perp}$	2.055	2.060
$A_{\parallel}$ (G)	155	156
$\alpha^2$	0.659	0.321
$\beta^2$	0.220	0.474
$\gamma^2$	0.227	0.490
$K_{\parallel}$	0.145	0.152
$K_{\perp}$	0.149	0.157
$\lambda_{\text{max}}$ (nm)	705	712

Table 5. Electrochemical data for binuclear copper(II) complexes **1** and **2** in DMSO ( $3 \times 10^{-3}$  M) containing 0.1 M TBAP as a supporting electrolyte and acetonitrile data is given in small bracket.

Complex	$E_{pc1}$ (V)	$E_{pa1}$ (V)	$E_{pc2}$ (V)	$E_{pa2}$ (V)	$DE_{pc1}$ (V)	$DE_{pc2}$ (V)	$\Delta E_{Dpc}$ (V)	$E^1_{1/2}$ (V)	$E^2_{1/2}$ (V)	$K_{con}$
<b>1</b>	-0.012 (-0.050)	0.247	-0.262 (-0.461)	-0.161	0.080	-0.261	0.341	0.118	-0.211	$3.6 \times 10^5$
<b>2</b>	-0.026 (-0.063)	0.250	-0.314 (-0.413)	-0.255 -0.600	0.064	-0.256	0.320	0.112	-0.284	$4.9 \times 10^6$

Table 6. Antioxidant SOD activity,  $IC_{50}$  values and first order kinetic catalytic constants for **1** and **2**.

Complex	$IC_{50}$ ( $\mu$ mol)	SOD activity ( $\mu$ mol $^{-1}$ )	$k_{McCF}$ (mol L $^{-1}$ s $^{-1}$ ) $\times 10^4$	Reference
Vc	852	1.17	0.39	[55a]
[(L $^1$ )Cu( $\mu$ -CH $_3$ COO) $_2$ Cu(L $^1$ )]	35	28.57	9.50	[1f]
[(L $^1$ )Cu( $\mu$ -NO $_3$ ) $_2$ Cu(L $^1$ )]	26	38.46	12.79	[1f]
[Cu $_2$ ( $\mu$ -benzoato)(L $^2$ ) $_2$ ]NO $_3$ ·2H $_2$ O	38	26.31	8.75	[7c]
[Cu $_2$ ( $\mu$ -succinato)(L $^3$ ) $_2$ (H $_2$ O)]ClO $_4$	44	22.72	7.560	[7c]
[(L $^4$ )Cu-( $\mu$ -CH $_3$ COO) $_2$ Cu(L $^4$ )] 4,4-bipy	52	19.23	6.39	[53a]
[(L $^5$ )Cu-( $\mu$ -NO $_3$ ) $_2$ Cu(L $^5$ )]	58	17.24	5.73	[53a]
[Cu( $\mu$ -CH $_3$ COO)(L $^6$ ) $_2$ ·4H $_2$ O	37	27.02	8.99	[53b]
[Cu(L $^1$ )(NO $_3$ )( $\mu$ -2aminopyrazine)Cu(L $^1$ )(NO $_3$ ) $_2$ ·2H $_2$ O	15	66.67	22.17	[5c]
[Cu $_2$ ( $\mu$ -sulfato)(L $_2$ )(2H $_2$ O)]·1.5H $_2$ O <b>1</b>	35	28.57	9.50	This work
Cu $_2$ ( $\mu$ -succinato)(L)(HL)(H $_2$ O)]ClO $_4$ <b>2</b>	24	41.66	13.84	This work

$k_{McCF}$  were calculated by  $k_{McCF} = k_{NBT} \times [NBT]/IC_{50}$ ,  $k_{NBT}$  (pH; 7.8) =  $5.94 \times 10^4$  (mol L $^{-1}$ )-1s $^{-1}$ . L1 = N'-[phenyl(pyridin-2-yl)methylidene]benzohydrazone, L2=N'-[(E)-phenyl(pyridin-2-yl)methylidene]benzoylhydrazone and L3 = N'-[(E)-pyridin-2-ylmethylidene]benzoylhydrazone, L4=N'-[phenyl(pyridin-2-yl)methylidene]furan-2-carbohydrazide, L5 =(2E,4Z)-N,2-dimethylhepta-2,4,6-trienamide-1-phenyl-1-pyridin-2-ylmethanimine, L6 = N'-(pyridine-2-ylmethylene) acetohydrazide.